Arch. Pharm. Chem. Life Sci. 2016, *349*, 1–11

ARCH PHARM
Archiv der Pharmazie

Full Paper

Identification of Indole-Based Chalcones: Discovery of a Potent, Selective, and Reversible Class of MAO-B Inhibitors

Rani Sasidharan[1], Sreedharannair Leelabaiamma Manju[2], Gülberk Uçar[3], Ipek Baysal[3], and Bijo Mathew[4]**

[1] College of Pharmaceutical Science, Government T.D. Medical College, Alappuzha, Kerala, India
[2] Organic Chemistry Division, SAS, VIT University, Vellore, Tamil Nadu, India
[3] Faculty of Pharmacy, Department of Biochemistry, Hacettepe University, Sıhhiye, Ankara, Turkey
[4] Division of Drug Design and Medicinal Chemistry Research Lab, Department of Pharmaceutical Chemistry, Ahalia School of Pharmacy, Palakkad, Kerala, India

A series of 11 indole-based chalcones (**IC1–11**) with various electron donating and withdrawing groups at the *para* position of the phenyl ring B were synthesized. All the compounds were tested for their human monoamine oxidase (hMAO)-A and hMAO-B inhibitory potencies. Most of the synthesized candidates proved to be potent and selective inhibitors of MAO-B rather than MAO-A, with a reversible and competitive mode. Among them, compound **IC9** was found to be a potent inhibitor of hMAO-B with $K_i = 0.01 \pm 0.005\,\mu M$ and a selectivity index of 120. It was found to be better than the standard drug, selegiline (hMAO-B with $K_i = 0.20 \pm 0.020\,\mu M$) with a selectivity index of 30.55. PAMPA assays were carried out for all the compounds in order to evaluate the capacity of the compounds to cross the blood–brain barrier. Moreover, the most potent MAO-B inhibitor, **IC9**, was nontoxic at 5 and 25 μM, with 95.20 and 69.17% viable cells, respectively. The lead compound **IC9** has an antioxidant property of 1.18 Trolox equivalents by ABTS assay. Molecular modeling studies were performed against hMAO-B to observe binding site interactions of the lead compound.

Keywords: 3-Acetyl indole / Chalcones / MAO / MAO-B / Molecular docking

Received: April 1, 2016; Revised: June 3, 2016; Accepted: June 3, 2016

DOI 10.1002/ardp.201600088

Additional supporting information may be found in the online version of this article at the publisher's web-site.

Introduction

Monoamine oxidases A and B (MAO-A and MAO-B) are flavin adenine dinucleotide (FAD) dependent enzymes found in the outer mitochondrial membrane in neuronal, glial, and other mammalian cells [1]. Both these enzymes catalyze the two-electron oxidation of biogenic amine substrates at the α-carbon and the reduced FAD is re-oxidized by molecular oxygen to yield hydrogen peroxide, while the imine product is in most instances hydrolyzed to the corresponding aldehyde [2, 3]. Particularly, MAO-A enzyme is responsible for the deamination of the epinephrine, norepinephrine, and serotonin, whereas the MAO-B enzyme metabolizes β-phenethylamine [4]. Due to their fundamental role in neurotransmitter metabolism, these isoforms are considered as attractive drug targets for mood disorders and neurodegenerative diseases [5]. In fact, MAO-A inhibitors are frequently used as antidepressants and antianxiety agents, while MAO-B inhibitors are relevant tools in the therapy of Alzheimer's and Parkinson's diseases as adjuvants to L-Dopa, the metabolic precursor of dopamine [6].

Correspondence: Dr. S. L. Manju, Associate Professor, Department of Chemistry, School of Advanced Sciences, VIT University, Vellore, Tamil Nadu, India, 632014.
E-mail: slmanju@vit.ac.in
Fax: 04162243092

*Additional correspondence: Prof. Dr. Gülberk Uçar, E-mail: gulberk@hacettepe.edu.tr;
Bijo Mathew, E-mail: bijovilaventgu@gmail.com.

Currently, clinically used human MAO-B inhibitors behave as selective and irreversible inhibitors. These candidates display the typical drawbacks of long-lasting enzyme inhibition, namely, *de novo* enzyme biosynthesis in the human brain and potential immunogenicity of enzyme-inhibitor adducts, high efficiency to target disruption, less sensitivity toward pharmacokinetic parameters, and increased duration of action. In general reversible inhibitors have safer profiles [7]. As the general body of information grows, it is sensible to continue to design new hMAO-B inhibitors to be used as neuroprotectant therapeutics with higher selectivities and fewer deleterious side effects.

Chalcones are open chain flavonoidal class of compounds consisting of two rings A and B separated by α, β-unsaturated carbonyl system. In this system, A ring is nearer to the carbonyl group and B ring is nearer to the β-carbon [8]. The first time MAO inhibitory activity of isolated isoliquiritigenin (natural chalcone) from the roots of *Glycyrrhiza uralensis* was done by Tanka et al. The inhibitory action of this chalcone was investigated by using the mitochondrial MAO of rat liver as the source of the enzyme [9, 10]. Their research set the stage for the chalcone family toward MAO recognition. Based upon the above observation, many of the research groups have explored the importance of electron withdrawing and electron donating motifs at various positions of A and B rings of chalcones and evaluated their MAO inhibition. The most active chalcones were characterized by the presence of hydroxyl and methoxyl groups at *ortho* and *para* positions, respectively, on the phenyl A ring and the lipophilic group such as such as chlorine, fluorine, and trifluoromethyl at *para* position on the B ring [11–15]. In addition, the incorporation of heteronucleus such as furan, chromene, piperidine, pyrrole, quinoline, and thiophene in the chalcone scaffold, also validated as MAO-A and -B inhibitors [16–23].

Many of the studies clearly revealed that chalcone compounds showed selective, reversible/irreversible, and potent MAO-B inhibition than MAO-A [24]. Recently, our group reported potent, selective, and reversible hMAO-B inhibitory properties of methoxylated and thienyl chalcones. Molecular modeling studies of these chalcones in the hMAO-B active site showed that the A ring of the ligand oriented toward the FAD co-factor and is stabilized by hydrogen bonds and hydrophobic interactions with Tyr398 and Tyr435 residues. Moreover the substituted B ring of chalcones are lined with the "entrance cavity" of MAO-B [13, 21–23].

With the aim to further explore the structure–activity relationships (SARs) of MAO inhibition by chalcone derivatives, we planned the introduction of indole ring system in the A ring with a variety of electron donating and withdrawing groups at the *para* position of phenyl ring B. The information regarding the exploration of various groups at the *para* position of ring B system of indole-based chalcone and its effect of MAO inhibition is not explored so far. 3-Acetyl indole moiety was selected as starting reagent for the synthesis of various indole-based chalcones, since indole is often present in compounds with remarkable MAO inhibitory activities [25–29]. Accordingly to these results, in this work we describe the synthesis, biological evaluation, and molecular modeling of indole-based chalcone derivatives as selective MAO-B inhibitors. The pharmacological profiles of these compounds including MAO-A and MAO-B inhibition, the kinetics and reversibility of enzyme inhibition, blood–brain barrier permeation, and cytotoxicity and antioxidant effects were evaluated.

Results and discussion

Chemistry

The synthetic strategy of indolyl chalcones is outlined in Scheme 1. The commercially available 3-acetyl indole and various *para*-substituted benzaldehydes underwent Claisen–Schmidt condensation in the presence of a base followed by acidification with dil. HCl to afford corresponding indolyl chalcones (**IC1–11**). The chemical structures of the compounds have been ascertained by means of their ^{1}H NMR, mass spectroscopic data, and elemental analysis. ^{1}H NMR spectrum showed different type of protons corresponding to the signals of the α,β- unsaturated unit, indole, and the mono-substituted phenyl system. It has been noted that the upfield proton of α-carbon and downfield proton of β-carbon coupled with methine proton with coupling constants 15.2–15.8 Hz. The large coupling constants suggest the presence of *trans* configuration in the indolyl chalcones. The protons belonging to the aromatic ring and indole ring are observed with the expected chemical shift and integral value. The

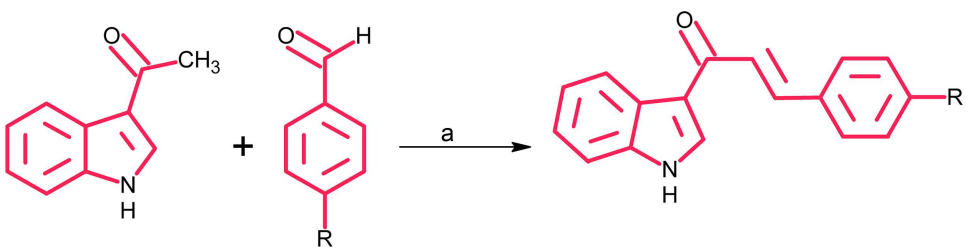

Scheme 1. Synthesis of indolyl chalcones. Reagents and conditions: (a) C_2H_5OH, 10% NaOH, reflux, 12–15 h.

characteristic peaks were observed in the mass spectra of the synthesized compounds. The presence of chlorine and bromine atom in the compounds of **IC8** and **IC9** showed characteristic [M+2] isotope peaks.

Pharmacological evaluation

MAO inhibition studies

To determine the inhibitory activities of the indole-based chalcones, the recombinant human MAO-A and MAO-B enzymes were used as enzyme sources and the activity was determined according to a previously published protocol using the Amplex Red MAO assay kit [30–32]. A reversible and selective hMAO-A inhibitor, moclobemide, and an irreversible (suicide) and selective hMAO-B inhibitor, selegiline were employed as the positive control compounds in this test. Compounds and reference inhibitors were independently treated with Amplex Red reagent before the experiment. None of them interfered with the measurements. Test compounds either did not interact with resorufin since the fluorescence signal did not change when the test and reference compounds were treated with various concentrations of resorufin. Specific enzyme activities were calculated as 164.99 ± 11.00 pmol/mg/min (n = 3) for hMAO-A and 141.20 ± 6.89 pmol/mg/min (n = 3) for hMAO-B. The calculated and experimental results are shown in Table 1. Selectivity indexes (SI) were expressed as K_i(MAO-A)/K_i(MAO-B). Selectivity toward MAO-A increases as the corresponding SI decreases.

It can be seen from Table 1 that all the tested compounds showed much better inhibitory activities against hMAO-B than hMAO-A except compound **IC7** which inhibited hMAO isoforms non-selectively, appeared as moderate to good inhibitors of hMAO-B with K_i values in the submicromolar range. Among these derivatives, compound **IC9** exhibited potent activity and higher selectivity toward hMAO-B with K_i and SI values of 0.01 ± 0.005 μM and 120. It was found to be 20-folds more efficient than the standard drug, selegiline (hMAO-B with $K_i = 0.20 \pm 0.020$ μM) with selectivity index of 30.55. This inhibitory activity in nanomolar range indicated that the crucial role of substituent at the *para* position of the phenyl ring B might be important for the hMAO-B activity and selectivity.

In general, variation of substituents in the *para* position of phenyl B ring system attempted in the heteroaryl chalcone scaffold resulted in improved inhibitory activity. In particular, the enhancement of lipophilicity (compounds **IC1–IC11**) by incorporating an electron donating lipophilic groups or bulky halogen at the *para* position on phenyl B ring system of

Table 1. hMAO inhibitory activities of indole-based chalcones.

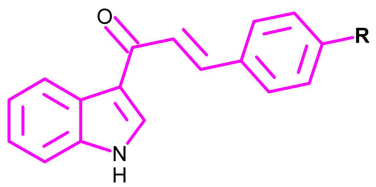

Compounds	R	Experimental K_i value (μM)[a]		Experimental SI[b]	Inhibition type	Reversibility	MAO selectivity
		MAO-A	MAO-B				
IC1	4–H	1.50 ± 0.09	0.14 ± 0.010	10.71	Competitive	Reversible	MAO-B
IC2	4–OH	1.98 ± 0.11	0.35 ± 0.021	5.66	Competitive	Reversible	MAO-B
IC3	4–OCH_3	1.20 ± 0.09	0.11 ± 0.009	10.91	Competitive	Reversible	MAO-B
IC4	4–CH_3	1.40 ± 0.10	0.09 ± 0.004	15.55	Competitive	Reversible	MAO-B
IC5	4–$N(CH_3)_2$	0.80 ± 0.04	0.15 ± 0.009	5.33	Competitive	Reversible	MAO-B
IC6	4–CH_2CH_3	0.74 ± 0.03	0.11 ± 0.007	6.73	Competitive	Reversible	MAO-B
IC7	4–NO_2	0.32 ± 0.01	0.30 ± 0.010	1.07	Competitive	Reversible	Non-selective
IC8	4–Cl	1.00 ± 0.07	0.28 ± 0.019	3.57	Competitive	Reversible	MAO-B
IC9	4–Br	1.20 ± 0.11	0.01 ± 0.005	120	Competitive	Reversible	MAO-B
IC10	4–F	2.90 ± 0.15	0.30 ± 0.020	9.66	Competitive	Reversible	MAO-B
IC11	4–CF_3	1.50 ± 0.11	0.19 ± 0.009	7.90	Competitive	Reversible	MAO-B
Moclobemide	–	0.17 ± 0.020	1.68 ± 0.110	0.10	Competitive	Reversible	MAO-A
Selegiline	–	6.11 ± 0.331	0.20 ± 0.020	30.55	Suicide inhibitor	Irreversible	MAO-B

[a] Value represents the mean ± SEM of three independent experiments.
[b] Selectivity index. It was calculated as K_i(MAO-A)/K_i(MAO-B). Selectivity toward MAO-A increases as the corresponding SI decreases while selectivity toward MAO-B isoform increases as the corresponding SI increases.

indolylchalcolones resulted in improved inhibitory activity against the MAO-B isozyme. The potential hMAO-B inhibitory activity and selectivity can be attributed to the presence of a 4-bromo substituent on the phenyl system (**IC9**). Presence of halogen such as chlorine or fluorine atom of phenyl ring showed almost similar results of MAO-B inhibition with K_i value of 0.28 and 0.30 μM, respectively. The presence of hydrophilic groups, like hydroxyl on the phenyl B ring led to a 35-fold decrease in potency ($K_i = 0.35$ μM) in **IC2** compared to the corresponding bromo derivative **IC9** against hMAO-B. The following ranking order of MAO inhibitory activity was observed for the indole-based chalcones as per experimental inhibitory data:

hMAO-A: 4-NO_2 > 4-C_2H_5 > 4-N-$(CH_3)_2$ > 4-Cl > 4-OCH_3 > 4-Br > 4-CH_3 > 4-CF_3 > 4-H > 4-OH > 4-F

hMAO-B: 4-Br > 4-CH_3 > 4-C_2H_5 > 4-OCH_3 > 4-H > 4-N-$(CH_3)_2$ > 4-CF_3 > 4-Cl > 4-NO_2 > 4-F > 4-OH

Thus, substitution with lipophilic motifs such as bromo, methyl, ethyl, and methoxyl groups at the *para* position on the phenyl ring B increased the potency toward hMAO-B compared to standard selegiline. This behavior is exemplified by **IC9** ($K_i = 0.01$ μM), **IC4** ($K_i = 0.09$ μM), **IC6** ($K_i = 0.11$ μM), and **IC3** ($K_i = 0.11$ μM). Among the non-functionalized phenyl ring compound **IC1** showed K_i value of 0.14 μM against hMAO-B, which further supports the above observation claiming the crucial role of the nature of the lipophilic *para* substitution on phenyl ring for the development of potent hMAO-B inhibitory activity. The potent chalcones from this series have been used as promising intermediates in the synthesis of 2-pyrazoline derivatives as part of an effort to discover novel MAO inhibitors [33]. Another motivating aspect is the inhibitory capacity **IC7** compound which showed K_i value of 0.30 and 0.32 μM toward both MAO-B and -A, respectively. It is to be noted that dual-target-directed MAO-B and MAO-A inhibitors may have enhanced therapeutic value, making such compounds ideal adjuvants to L-DOPA treatment in Parkinson's disease, particularly when associated with depressive state of mood disorders [34].

Kinetic studies

Kinetic analyses were carried out for most potent MAO-B inhibitor **IC9** from this series to gain the further insight into the mode of MAO inhibition. A set of Lineweaver–Burk plots was constructed in the absence and presence of various concentrations of compound **IC9**. The set consisted of five graphs, each constructed by measuring MAO-B and MAO-A catalytic rate at different substrate concentrations (0.01–0.15 μM). The observation that the lines were linear and intersect on the *y*-axis suggests that **IC9** interacts with the catalytic site of hMAO-B, with a competitive mode of inhibition (Fig. 1). The replots of the slopes of the Lineweaver–Burk plots versus inhibitor concentration are shown in Fig. 2 and the K_i was estimated as 0.012 μM for **IC9** (hMAO-B).

Reversibility studies

Newly synthesized indole-based chalcone derivatives inhibited the hMAO isoforms reversibly. Table 2 presents the reversibility of hMAO-B inhibition with the novel compounds. The reversibility of MAO inhibition by the new compounds was investigated by determination of the recoveries of MAO

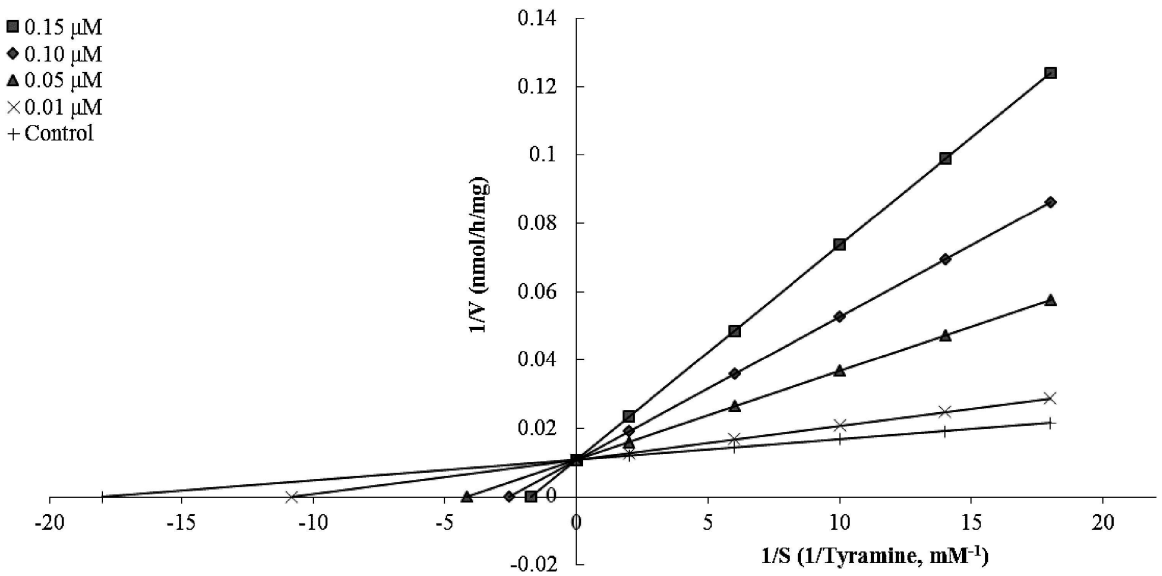

Figure 1. Lineweaver–Burk plots of hMAO-B activity in the absence and presence of various concentrations of compound **IC9**.

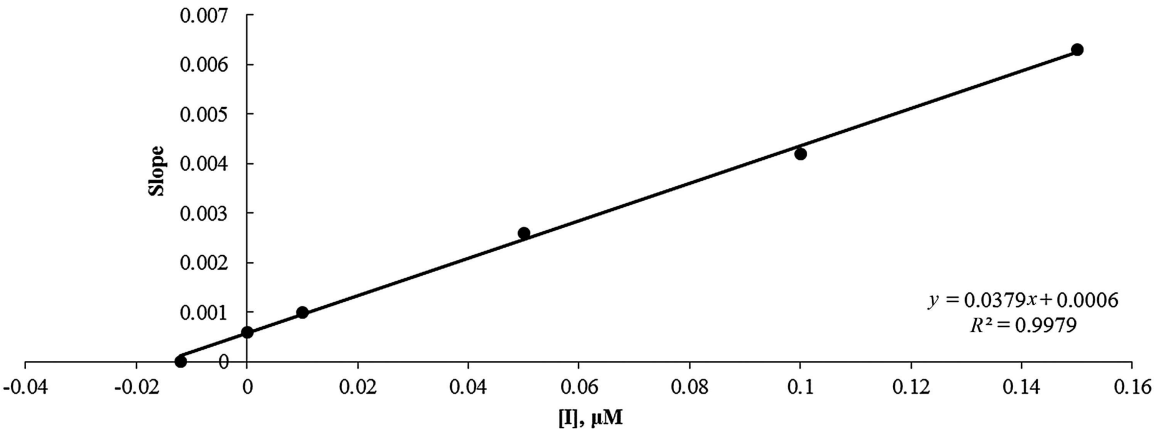

Figure 2. Replots of the slopes of the Lineweaver–Burk plots versus inhibitor **IC9** concentration (hMAO-B).

activity after dialysis of enzyme-inhibitor mixtures. MAO isoforms were incubated in the presence of the inhibitors, at concentrations equal to $4 \times IC_{50}$, for a period of 15 min and subsequently dialyzed for 24 h. hMAO-B inhibition by compound **IC9** was completely reversed after 24 h of dialysis. Results suggest that newly synthesized indolylchalcones are reversible inhibitors of hMAO isoforms and have considerable advantages compared to irreversible inhibitors which may possess serious pharmacological side effects. The potent and selective MAO-B inhibitor selegiline has been reported to have severe side effects due to its amphetamine metabolites and both selegiline and rasagiline are irreversible MAO-B inhibitors triggering pharmacological side effects in long term treatment of Parkinson's disease [35]. Reversibility of hMAO-B inhibition with compound **IC9** was found to be good in the present series. The reversiblity of compound **IC9** was calculated as 28.10 ± 1.56 and 96.00 ± 3.13 before and after dialysis, respectively.

In vitro blood–brain barrier permeation assay

Newly synthesized derivatives were screened for their ability to cross the blood–brain barrier (BBB) since this is the first requirement for the design of successful CNS drugs. To investigate whether the present compounds could pass this barrier, a widely known parallel artificial membrane permeation assay of blood–brain barrier (PAMPA-BBB) was used. Assay validation was made by comparing experimental permeabilities of nine commercial drugs with reported values (Table 3). A plot of experimental data versus bibliographic values gave a good linear correlation ($R^2 = 0.9965$, Fig. 3).

Table 2. Reversibility of the inhibition of hMAOs by indole-based chalcones.

Test compounds incubated with hMAO	hMAO-A activity before washing (%)	hMAO-A activity after washing (%)	hMAO-B activity before washing (%)	hMAO-B activity after washing (%)	Reversibility
IC1	90.25 ± 3.77	94.00 ± 4.61	40.55 ± 1.96	90.44 ± 3.27	Reversible
IC2	87.20 ± 3.60	91.25 ± 3.05	51.20 ± 2.30	88.27 ± 2.37	Reversible
IC3	89.55 ± 4.75	88.20 ± 3.78	42.20 ± 2.10	94.00 ± 3.25	Reversible
IC4	90.66 ± 4.05	88.22 ± 4.00	40.00 ± 2.01	87.55 ± 4.09	Reversible
IC5	90.01 ± 3.55	92.78 ± 4.00	55.00 ± 2.16	92.39 ± 4.23	Reversible
IC6	87.44 ± 4.00	92.26 ± 4.50	52.98 ± 2.44	94.00 ± 4.01	Reversible
IC7	50.68 ± 2.66	88.21 ± 4.00	49.88 ± 2.02	90.32 ± 4.03	Reversible
IC8	88.21 ± 4.00	93.06 ± 3.74	53.20 ± 4.05	90.47 ± 3.33	Reversible
IC9	95.20 ± 5.00	94.60 ± 3.55	28.10 ± 1.56	96.00 ± 3.13	Reversible
IC10	94.78 ± 4.20	95.55 ± 4.30	51.28 ± 3.16	95.00 ± 2.85	Reversible
IC11	89.99 ± 2.60	92.40 ± 3.22	50.22 ± 2.16	95.80 ± 2.56	Reversible
With no inhibitor	100 ± 0.00	100 ± 0.00	100 ± 0.00	100 ± 0.00	–
Moclobemide	45.56 ± 3.02	89.25 ± 3.77	99.00 ± 4.87	94.89 ± 5.22	Reversible
Selegiline	92.21 ± 3.90	90.05 ± 5.552	51.00 ± 3.41	52.09 ± 3.00	Irreversible

Each value represents the mean ± SEM (n = 3).

Table 3. Permeability (*Pe* 10^{-6} cm s^{-1}) in the PAMPA-BBB assay for commercial drugs used in the validation of the assay and for indole-based chalcones.

Compounds[a)]	Bibliography *Pe* ($\times 10^{-6}$ cm s^{-1})[b)]	Experimental *Pe* ($\times 10^{-6}$ cm s^{-1})[c)]	Prediction
IC1		10.55 ± 1.05	CNS+
IC2		9.04 ± 0.54	CNS+
IC3		12.87 ± 1.05	CNS+
IC4		14.02 ± 1.10	CNS+
IC5		8.88 ± 0.39	CNS+
IC6		9.00 ± 0.45	CNS+
IC7		4.11 ± 0.16	CNS+
IC8		6.22 ± 0.51	CNS+
IC9		15.27 ± 1.09	CNS+
IC10		10.02 ± 0.98	CNS+
IC11		9.57 ± 0.52	CNS+
Testosterone	17.0	16.72 ± 1.52	CNS+
Verapamil	16.0	14.97 ±1.65	CNS+
β-Estradiol	12.0	10.72 ± 1.69	CNS+
Progesterone	9.3	7.88 ± 0.33	CNS+
Corticosterone	5.1	4.08 ± 1.03	CNS+
Piroxicam	2.5	2.23 ± 0.53	CNS+/–
Hydrocortisone	1.8	1.53 ± 0.48	CNS–
Lomefloxacin	1.1	1.09 ± 0.23	CNS–
Dopamine	0.2	0.36 ± 0.14	CNS–

[a)] Compounds were dissolved in DMSO at 5 mg/mL and diluted with PBS/EtOH (70:30). The final concentration of compounds was 100 μg/mL.
[b)] Taken from [36].
[c)] Values were expressed as the mean ± SEM of three independent experiments.

According to the limits established by Di et al. for blood–brain barrier permeation [36], test compounds were classified as follows:

CNS + (high BBB permeation predicted): $Pe(10^{-6}\,\mathrm{cms}^{-1}) > 4.00$

CNS − (low BBB permeation predicted): $Pe(10^{-6}\,\mathrm{cms}^{-1}) < 2.00$

CNS ± (BBB permeation uncertain): $Pe(10^{-6}\,\mathrm{cms}^{-1})$ from 4.00 to 2.00

The data showed in Table 3 indicated that all of the indole-based chalcones can cross the BBB to target the enzyme in the central nervous system. Compounds **IC9**, **IC4**, and **IC3** showed the highest permeability suggesting that they may cross the BBB easily and reach the biological targets located in the CNS, which was consistent with our design strategy.

Cytotoxicity studies

The toxicities of the newly synthesized derivatives were determined in order to obtain data for the assessment of their possible drug-like properties. *In vitro* cytotoxicity of the novel compounds was tested in HepG2 cells at three different concentrations (1–25 μM) (Table 4). The results showed that almost all of the novel compounds were not toxic to hepatic cells at 1 μM concentration. At 5 μM, compounds **IC3**, **IC4**, **IC9**, and **IC10** were found to be completely nontoxic to the cells. The most potent MAO-B inhibitor **IC9** in the current study was nontoxic at 5 and 25 μM, with 95.20 and 69.17% viable cells, respectively.

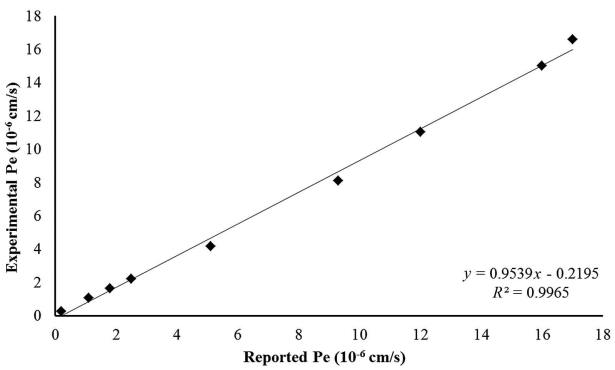

Figure 3. Linear correlation between experimental and reported permeability of commercial drugs using the PAMPA-BBB assay.

Table 4. ***In vitro*** **cytotoxicity test and ABTS assay for the indole-based chalcones.**

Compounds	Viability (%)			ABST assay[a)]
	1 μM	5 μM	25 μM	
IC1	88.22 ± 3.05*	62.49 ± 1.44**	58.23 ± 3.00**	0.48
IC2	97.55 ± 5.14	89.65 ± 2.75*	57.54 ± 1.44**	0.54
IC3	98.15 ± 1.86	95.77 ± 3.01	62.21 ± 1.47**	0.67
IC4	97.00 ± 2.98	94.89 ± 3.55	60.87 ± 2.17**	0.73
IC5	97.84 ± 5.53	82.58 ± 1.26**	73.38 ± 1.22**	0.68
IC6	96.80 ± 3.87	56.58 ± 1.71**	56.58 ± 1.71**	0.58
IC7	96.00 ± 2.85	56.31 ± 1.87**	53.16 ± 0.93***	0.32
IC8	85.21 ± 2.56*	63.64 ± 0.68**	52.28 ± 1.46***	0.80
IC9	97.86 ± 4.45	95.20 ± 3.11	69.17 ± 0.60**	1.18
IC10	96.88 ± 2.74	95.22 ± 2.15	74.57 ± 0.97**	1.32
IC11	96.54 ± 3.78	84.33 ± 2.55*	65.80 ± 1.99**	0.35

Data were expressed as mean ± SEM ($n = 3$). Cell viability was expressed as a percentage of the control value. $p < 0.05$ was considered as statistically significant. ($^{*}p < 0.05$, $^{**}p < 0.01$, $^{***}p < 0.001$ vs. control).
[a)]Data were expressed as Trolox equivalent (mmol Trolox)/(mmol tested compound).

ABTS radical cation scavenging assay

Compounds **IC1–11** were tested for their antioxidant activities by using the 2,2′-azino-bis-2-ethybenz-thiazoline-6-sulfonic acid (ABTS) method. Trolox (a water-soluble vitamin E analog) was used as a reference standard [37, 38]. Their antioxidant activities were provided as a Trolox equivalent, with their relative potency at 25 mM compared with Trolox. As shown in Table 4, compounds **IC8**, **IC9**, and **IC10** had the ability to scavenge the ABTS radical with 0.80, 1.18, 1.32 Trolox equivalents, respectively. The most active compounds were observed for the compounds with halogen substitution at the *para* position on ring B of indolyl chalcones. However, electron withdrawing group such as nitro and trifluoromethyl substitution on the phenyl ring were unfavorable to the ABTS radicals scavenging activity.

Computational studies

Molecular docking studies

To investigate the hypothetical molecular mechanism of hMAO-B inhibition by the lead compound **IC9**, molecular docking studies were carried out using AutoDock4.2. In hMAO-B, either substrates or competitive inhibitors bind to hydrophobic cavity which includes: an "entrance cavity" lined with Ile199 and the "substrate cavity". Here smaller entrance cavity with Ile199 effectively serves as a gate between these cavities. Depending on the structure of the bound inhibitor, the two cavities may be either separate or fused [39, 40]. The bromo-substituted phenyl ring of **IC9** is oriented horizontally sandwiched between the phenolic side chains of Tyr435 and Tyr398 residues, and it approached from the *re* face of FAD making one π–π stacking interaction with Tyr435 in the active site of hMAO-B. The interaction of **IC9** is also stabilized by one more π–π stacking interaction of carbocyclic ring of indole with the FAD along with one intermolecular hydrogen bond was observed between the NH group of indole and the Tyr325 (Fig. 4).

Conclusion

From inspection of the chemical structures, it can be concluded that among the synthesized compounds, the

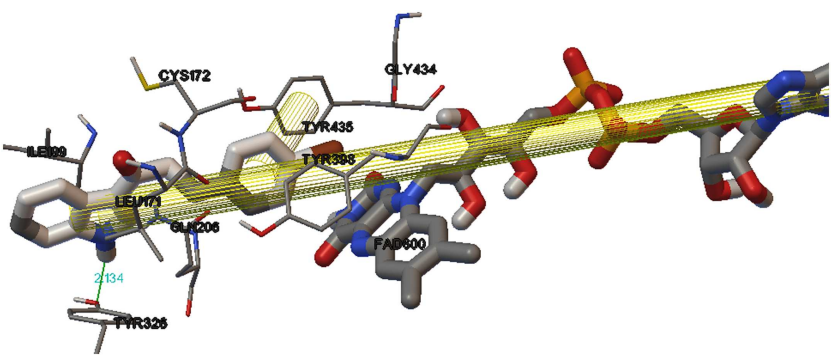

Figure 4. Docking pose of **IC9** in the MAO-B active site: Yellow mesh indicates π–π stacking interaction and blue line indicates H-bonding interaction.

hMAO-B inhibitory activity was strongly affected by the size and nature of the substituent groups at the *para* position on the phenyl ring of indolyl chalcones. This study highlighted the importance of bromine atom at the *para* position on phenyl ring that could significantly enhance the hMAO-B inhibitory activities of indolyl chalcones. The K_i value of hMAO-B inhibition of the compounds ranges from 0.01 to 0.35 μM, with compound **IC9** being the most potent and more efficient than the standard selegiline. Besides, this compound is good antioxidant with brain penetration capacity for CNS activity. In the cell viability, **IC9** was shown to have very low toxicity in HepG2 cells and showed good hepato protective action. Altogether, the multifunctional effects of this indolyl derivative qualify them as potential selective and reversible type of hMAO-B inhibitor and might be promising lead candidates for further research for the development of anti-Parkinson's agents.

Experimental

Chemistry

General

3-Acetyl indole and all the aromatic benzaldehydes were procured from Sigma–Aldrich, USA. Melting points of all the synthesized derivatives were determined by open-capillary tube method and values were uncorrected. Proton (^{1}H) nuclear magnetic resonance (NMR) spectra were recorded on a Bruker Avance III 600 spectrometer at frequency of 400 MHz (Bruker, Karlsruhe, Germany). All NMR measurements were conducted in $CDCl_3$, and the chemical shifts are reported in parts per million (δ) downfield from the signal of tetramethylsilane added to the deuterated solvent. Mass spectra were recorded on a JEOL GCmate mass spectrometer. Elemental analyses (C, H, N) were performed on a Leco CHNS 932 analyzer.

The InChI codes of the investigated compounds are provided as Supporting Information.

*General procedure for the synthesis of **IC1–11***

To a solution of 3-acetylindole (1 mmol) and appropriate aldehyde (1 mmol) in ethanol (20 mL) was added 10% sodium hydroxide (2 mL) and refluxed the reaction mixture for 15 h. The contents of reaction mixture were poured into ice-cold water and neutralized with dilute hydrochloric acid. The solid so obtained was filtered, dried, and recrystallized from suitable solvent to afford (**IC1–11**) [41].

*(2E)-1-(1H-Indol-3-yl)-3-phenylprop-2-en-1-one (**IC1**)*

Pale white, yield: 40%, m.p. 173–175°C. ^{1}H NMR (400 MHz, DMSO) δ ppm: ^{1}H NMR (400 MHz, DMSO) δ ppm: 7.21 (d, 1H, $J = 14.4$ Hz, Hα), 7.13–7.45 (m, 4H, Ar-H), 7.49 (d, 1H, $J = 15.6$ Hz, $H_β$), 8.19–8.45 (m, 4H, Ar-H), 11.98 (s, 1H, NH): ESI-MS (*m/z*): calculated 247.267, observed 247.291 $[M+]^+$. Anal. calcd. for $C_{17}H_{13}NO$: C, 82.57; H, 5.30; N, 5.66. Found: C, 82.68; H, 5.34; N, 5.86.

*(2E)-3-(4-Hydroxyphenyl)-1-(1H-indol-3-yl)prop-2-en-1-one (**IC2**)*

Pale brown, yield: 45%, m.p. 210–212°C. ^{1}H NMR (400 MHz, DMSO) δ ppm: 5.22 (s, 1H, OH), 7.19 (d, 1H, $J = 14.4$ Hz, Hα), 7.19–7.31 (m, 3H, Ar-H), 7.47 (d, 1H, $J = 15.6$ Hz, $H_β$), 8.17–8.30 (m, 4H, Ar-H), 11.91 (s, 1H, NH): ESI-MS (*m/z*): calculated 263.290, observed 263.222 $[M+]^+$. Anal. calcd. for $C_{17}H_{13}NO_2$: C, 77.55; H, 4.98; N, 5.32. Found: C, 77.63; H, 4.86; N, 5.46.

*(2E)-1-(1H-Indol-3-yl)-3-(4-methoxyphenyl)prop-2-en-1-one (**IC3**)*

Pale yellow, yield: 52%, m.p. 202–204°C. ^{1}H NMR (400 MHz, DMSO) δ ppm: 3.86 (s, 3H, OCH_3), 6.92–7.79 (m, 9, Ar-H), 7.21 (d, 1H, $J = 15.6$ Hz, $CH_α$), 7.83(d, 1H, $J = 15.6$ Hz, $CH_β$), 10.80 (s, 1H, NH): ESI-MS (*m/z*): calculated 277.317, observed 277.270 $[M+]^+$. Anal. calcd. for $C_{18}H_{15}NO_2$: C, 77.96; H, 5.45; N, 5.05. Found: C, 77.93; H, 5.46; N, 5.02.

*(2E)-1-(1H-Indol-3-yl)-3-(4-methylphenyl)prop-2-en-1-one (**IC4**)*

Pale yellow, yield: 51%, m.p. 208–210°C. ^{1}H NMR (400 MHz, DMSO) δ ppm: 3.41 (s, 3H, CH_3), 6.81–7.76 (m, 9, Ar-H), 7.36 (d, 1H, $J = 15.6$ Hz, $CH_α$), 7.95 (d, 1H, $J = 15.6$ Hz, $CH_β$), 11.08 (s, 1H, NH): ESI-MS (*m/z*): calculated 261.317, observed 261.278 $[M+]^+$. Anal. calcd. for $C_{18}H_{15}NO$: C, 82.73; H, 5.79; N, 5.36. Found: C, 82.83; H, 5.81; N, 5.22.

*(2E)-3-[4-(Dimethylamino)phenyl]-1-(1H-indol-3-yl)prop-2-en-1-one (**IC5**)*

Orange, yield: 61%, m.p. 195–197°C. ^{1}H NMR (400 MHz, DMSO) δ ppm: 3.13 (s, 6H, $N(CH_3)_2$), 6.89–7.92 (m, 9, Ar-H), 6.92. (d, 1H, $J = 15.2$ Hz, $CH_α$), 7.85 (d, 1H, $J = 15.6$ Hz, $CH_β$), 11.08 (s, 1H, NH): ESI-MS (*m/z*): calculated 290.359, observed 290.996 $[M+]^+$. Anal. calcd. for $C_{18}H_{18}N_2O$: C, 78.59; H, 6.25; N, 9.65. Found: C, 78.39; H, 6.80; N, 9.72.

*(2E)-3-(4-Ethylphenyl)-1-(1H-indol-3-yl)prop-2-en-1-one (**IC6**)*

Brown, yield: 51%, m.p. 198–200°C. ^{1}H NMR (400 MHz, DMSO) δ ppm: 1.43 (t, 3H, CH_3), 2.91 (q, 2H, CH_2), 6.82 (d, 1H, $J = 16.0$ Hz, $CH_α$), 6.93–7.97 (m, 9, Ar-H), 7.84 (d, 1H, $J = 15.6$ Hz, $CH_β$), 11.18 (s, 1H, NH): ESI-MS (*m/z*): calculated 275.344, observed 275.029 $[M+]^+$. Anal. calcd. for $C_{19}H_{17}NO$: C, 82.88; H, 6.22; N, 5.09. Found: C, 82.83; H, 6.24; N, 5.12.

*(2E)-1-(1H-Indol-3-yl)-3-(4-nitrophenyl)prop-2-en-1-one (**IC7**)*

Yellow, yield: 58%, m.p. 212–214°C. ^{1}H NMR (400 MHz, DMSO) δ ppm: 6.91 (d, 1H, $J = 16.0$ Hz, $CH_α$), 6.83–7.99 (m, 9, Ar-H), 7.73 (d, 1H, $J = 15.6$ Hz, $CH_β$), 11.21 (s, 1H, NH): ESI-MS (*m/z*): calculated 292.289, observed 292.230 $[M+]^+$. Anal. calcd. for $C_{17}H_{12}N_2O_3$: C, 69.86; H, 4.14; N, 9.58. Found: C, 69.80; H, 4.24; N, 9.62.

*(2E)-3-(4-Chlorophenyl)-1-(1H-indol-3-yl)prop-2-en-1-one (**IC8**)*

Pale white solid, yield: 61%, m.p. 200–202°C. ^{1}H NMR (400 MHz, $CDCl_3$) δ ppm: 7.17–8.30 (m, 9, Ar-H), 8.17 (d, 1H,

$J = 15.6$ Hz, CH_α), 8.76 (d, 1H, $J = 15.6$ Hz, CH_β), 11.91 (s, 1H, NH); ESI-MS (*m/z*): calculated 281.736, observed 282.213 $[M+]^+$, [M+2]. Anal. calcd. for $C_{17}H_{12}ClNO$: C, 72.47; H, 4.29; N, 4.97. Found: C, 72.45; H, 4.94; N, 4.92.

*(2E)-3-(4-Bromophenyl)-1-(1H-indol-3-yl)prop-2-en-1-one (**IC9**)*
Dark yellow solid, yield: 73%, m.p. 180–182°C. ^{1}H NMR (400 MHz, $CDCl_3$) δ ppm: 6.66–7.78 (m, 9, Ar-H), 7.51 (d, 1H, $J = 16.0$ Hz, CH_α), 7.82 (d, 1H, $J = 16.0$ Hz, CH_β), 11.35 (s, 1H, NH); ESI-MS (*m/z*): calculated 326.187, observed 326.191 $[M+]^+$, [M+2]. Anal. calcd. for $C_{17}H_{12}BrNO$: C, 62.60; H, 3.71; N, 4.29. Found: C, 62.55; H, 3.84; N, 4.22.

*(2E)-3-(4-Fluorophenyl)-1-(1H-indol-3-yl)prop-2-en-1-one (**IC10**)*
Yellow solid, yield: 53%, m.p. 218–220°C. ^{1}H NMR (400 MHz, $CDCl_3$) δ ppm: 6.75–7.98 (m, 9, Ar-H), 7.59 (d, 1H, $J = 16.0$ Hz, CH_α), 7.92 (d, 1H, $J = 16.0$ Hz, CH_β), 11.29 (s, 1H, NH); ESI-MS (*m/z*): calculated 265.281, observed 265.243 $[M+]^+$. Anal. calcd. for $C_{17}H_{12}FNO$: C, 76.97; H, 4.56; N, 5.28. Found: C, 76.95; H, 4.64; N, 5.26.

*(2E)-1-(1H-Indol-3-yl)-3-[4-(trifluoromethyl)phenyl]prop-2-en-1-one (**IC11**)*
Pale brown, yield: 93%, m.p. 192–194°C. ^{1}H NMR (400 MHz, $CDCl_3$) δ ppm: 6.85–7.94 (m, 9, Ar-H), 7.49 (d, 1H, $J = 16.0$ Hz, CH_α), 7.86 (d, 1H, $J = 16.0$ Hz, CH_β), 11.41 (s, 1H, NH); ESI-MS (*m/z*): calculated 315.289, observed 315.289 $[M+]^+$. Anal. calcd. for $C_{17}H_{12}FNO$: C, 68.57; H, 3.84; N, 4.44. Found: C, 68.88; H, 3.80; N, 4.36.

Biological assays

Chemicals

Recombinant hMAO-A and hMAO-B (expressed in baculovirus-infected BTI insect cells), *R*-(−)-deprenyl hydrochloride (selegiline), moclobemide, resorufin, dimethyl sulfoxide (DMSO), and other chemicals were purchased from Sigma–Aldrich (Munich, Germany). The Amplex®-Red MAO assay kit (Mybiosource, USA) contained benzylamine, *p*-tyramine, clorgyline, pargyline, and horseradish peroxidase.

Determination of hMAO activity

hMAO activites were determined by a fluorimetric method described and modified previously using *p*-tyramine (0.05–0.50 mM) as common substrate [30–32]. Study medium contained 0.1 mL of sodium phosphate buffer (0.05 M, pH 7.4), various concentrations of the synthesized compounds or known inhibitors (moclobemide, selegiline, and lazabemide), and recombinant hMAO-A or hMAO-B. This mixture was incubated for 15 min at 37°C in microplates, placed in the dark fluorimeter chamber. Reaction was started by adding 200 μM Amplex Red reagent, 1 U/mL horseradish peroxidase (HRP), and *p*-tyramine. The production of H_2O_2 catalyzed by MAO isoforms was detected using Amplex®-Red reagent, in the presence of HRP to produce the fluorescent product resorufin. Resorufin was quantified at 370°C in a multidetection microplate fluorescence reader with excitation at 545 nm, and emission at 590 nm, over a 15 min period, in which the fluorescence increased linearly. The specific fluorescence emission was calculated after subtraction of the background activity, which was determined from wells containing all components except the hMAO isoforms, which were replaced by a sodium phosphate buffer solution. In our experimental conditions, this background activity was negligible.

Control experiments were carried out by replacing the compound and known inhibitors. The possible capacity of compounds to modify the fluorescence generated in the reaction mixture due to non-enzymatic inhibition was determined by adding these compounds to solutions containing only the Amplex Red reagent in a sodium phosphate buffer. The new compounds and reference inhibitors themselves did not react directly with Amplex® Red reagent. Newly synthesized compounds did not cause any inhibition on the activity of HRP in the test medium.

Kinetic studies

Synthesized compounds were dissolved in dimethyl sulfoxide, with a maximum concentration of 1% and used in a wide concentration range of 0.010–0.15 μM. The mode of MAO inhibition was examined using Lineweaver–Burk plotting. The slopes of the Lineweaver–Burk plots were plotted versus the inhibitor concentration and the K_i values were determined from the *x*-axis intercept as $-K_i$. Each K_i value is the representative of single determination where the correlation coefficient (R^2) of the replot of the slopes versus the inhibitor concentrations was at least 0.98. SI was calculated as K_i(hMAO-A)/K_i(hMAO-B). The protein was determined according to the Bradford method [42].

Reversibility of inhibition

Reversibility of the MAO inhibition with the compounds was determined by dialysis method previously described [43]. Dialysis tubing 16 × 25 mm (Sigma, Germany) with a molecular weight cut-off of 12000 and a sample capacity of 0.5–10 mL was used. Adequate amounts of the recombinant enzymes (hMAO-A or -B) (0.05 mg/mL) were incubated with a concentration equal to fourfold of the IC_{50} values for the inhibition of hMAO-A and -B, respectively, in potassium phosphate buffer (0.05 M, pH 7.4, 5% sucrose containing 1% DMSO) for 15 min at 37°C. Other sets were prepared by preincubation of same amount of hMAO-A and -B with the reference inhibitors (moclobemide and selegiline). Enzyme/inhibitor mixtures were subsequently dialyzed at 4°C in 80 mL of dialysis buffer (100 mM potassium phosphate, pH 7.4, 5% sucrose). The dialysis buffer was replaced with fresh buffer at 3 and 7 h after the start of dialysis. At 24 h after dialysis, residual MAO activities were measured. All reactions were carried out in triplicate and the residual enzyme catalytic rates were expressed as mean ± SEM. For comparison, undialyzed mixtures of the MAOs and the inhibitors were kept at 4°C over the same time period.

In vitro blood–brain barrier permeation assay
The ability of newly synthesized compounds to penetrate into brain was determined using a parallel artificial membrane permeation assay (PAMPA) for blood–brain-barrier according to a previous method [36]. Briefly, compounds and the commercial drugs were dissolved in DMSO at a concentration of 5 mg/mL. They were diluted with a mixture 70:30 of phosphate buffered saline solution and ethanol (PBS/EtOH) to give a final concentration of 25 μg/mL. The filter membrane in donor microplate was coated with porcine polar brain lipid (PBL) dissolved in dodecane (4 μL, 20 mg/mL). A total of 200 μL of diluted solution and 300 μL of PBS/EtOH (70:30) were added to the donor and the acceptor wells, respectively. The donor filter plate was carefully placed on the acceptor plate. Sandwich system was kept at 25°C for 16 h. The donor plate was carefully removed, and the concentrations of the compounds and the commercial drugs in the acceptor, donor, and reference wells were measured with a UV plate reader.

Cytotoxic activity
Cell viability was measured by quantitative colorimetric assay with 3-[4,5-dimethylthiazol-2-yl]-2,5-diphenyl-tetrazolium bromide (MTT) (Sigma–Aldrich). Human hepatoma cell line HepG2 (Invitrogen) was cultured in Dulbecco's Modified Eagle's Medium (DMEM) supplemented with 2 mM L-Glutamine, 10% heat-inactivated fetal bovine serum (FBS), 100 units/mL penicillin, and 100 μg/mL streptomycin. Cells were seeded in supplemented medium and maintained at 37°C in a humidified atmosphere of 5% CO_2 and 95% air. Exponentially growing HepG2 cells were subcultured in 96-well plates. The cells were treated with the novel compounds (1, 5, and 25 μM) or 0.1% DMSO as a vehicle control for 24 h. A total of 10 μL of the MTT labeling reagent, at a final concentration of 5 mg/mL, was added to each well at the end of the incubation time and the plate placed in a humidified incubator at 37°C with 5% CO_2 and 95% air (v/v) for 4 h until the appearence of purple formazan crystals formed. Then, the insoluble formazan was dissolved with 100 μL of dimethylsulfoxide (DMSO) by shaking 1 h in darkness. MTT reduction was measured at 590 nm. Control cells treated with 0.1% DMSO were used as 100% viability [44, 45]. Significance was determined using Student's *t*-test. Results were expressed as mean ± SEM. Differences are considered statistically significant at $p < 0.05$.

Antioxidant activity
The ABTS radical cation scavenging method can be described as follows: 2,2′-Azino-*bis*-2-ethylbenzthiazoline-6-sulfonic acid (ABTS) was dissolved in purified water to a 7 mM concentration. The ABTS radical cation ($ABTS^{\bullet+}$) was produced by reacting ABTS stock solution with 2.45 mM potassium persulfate (final concentration) and allowing the mixture to stand in the dark at room temperature for at least 18 h before use. The stock solution of ABTS was serially diluted with sodium phosphate buffer (50 mM, pH 7.4) to 100 mM. Trolox and all the target compounds at different concentrations (total volume of 50 mL) were added to 150 mL of 100 mM ABTS solution, respectively. After the addition of either Trolox or another antioxidant to the ABTS solution, complete mixing of the reactants was achieved by bubbling three to four times using plastic pipettes. The optical absorbance of ABTS at 415 nm was measured at 6 min after addition and equilibrated at 30°C. Each individual treatment was repeated three times and the results of the experiments were compared [37, 38].

Molecular docking studies

In the current molecular simulation study, AUTODOCK4.2 software was used to establish a ligand-based computer modeling program for the prediction of binding energy of the selected compounds with hMAO isoforms [46]. Docking protocol was done with X-ray crystal structure of hMAO-A (2BXR) and hMAO-B (2BYB) downloaded from Protein Data Bank (www.rcsb.org) [47]. Protein preparation was carried out using Protein Preparation Wizard of Maestro-8.5 (Schrodinger LLC) [48]. Ligands were prepared through PRODRG webserver (http://davapc1.bioch.dundee.ac.uk/cgi-bin/prodrg) [49]. The receptor grids for both enzymes were generated with following parameters: grid box dimension (*xyz*) of $60 \times 60 \times 60$; grid spacing of 0.375 Å and center of the grid box positioned on N5 atom of FAD (co-factor). The .gpf (grid parameter file) file generated through MGLTools-1.5.6 was then used to generate map types through autogrid4 execution file. Similarly for each ligand, a docking parameter file (.dpf) has been written using MGLTools-1.5.6 with default parameters except: no. of runs: 50; population size: 300, and number of evaluations set at medium. The Lamarckian genetic algorithm was selected for all molecular docking simulations. The .dpf file generated for each ligand was then used for running molecular docking simulation using autodock4 execution file, which will generate docking log file (*.dlg) containing results of the simulation. Through analyze module in MGLTool-1.5.6, the docking log files were analyzed. Top scoring molecule from the largest cluster was considered for analysis [50].

The authors are thankful to IIRBS, Mahatma Gandhi University, Kottayam and SAIF, IIT, Chennai, India for carrying out the spectral analysis.

The authors have declared no conflict of interest.

References

[1] K. F. Tipton, *Cell Biochem. Funct*. **1986**, *4*, 79–87.
[2] C. Binda, A. Mattevi, D. E. Edmondson, *Int. Rev. Neurobiol*. **2001**, *100*, 1–11.
[3] M. B. Youdim, Y. S. Bakhle, *Br. J. Pharmacol*. **2006**, *147*, S287–S296.
[4] P. Riederer, L. Lachenmayer, G. Laux, *Curr. Med. Chem*. **2004**, *11*, 2033–2043.
[5] R. R. Ramsay, *Curr. Pharm. Des*. **2013**, *19*, 2529–2439.

[6] D. E. Edmondson, *Curr. Pharm. Des*. **2014**, *20*, 155–160.
[7] S. Carradori, R. Silvestri, *J. Med. Chem*. **2015**, *58*, 6717–6732.
[8] B. Mathew, J. Suresh, S. Anbazhagan, J. Paulraj, G. K. Krishnan, *Biomed. Prev. Nutr*. **2014**, *4*, 451–458.
[9] S. Tanaka, Y. Kuwai, M. Tabata, *Planta Med*. **1987**, *53*, 5–8.
[10] T. Takeuchi, K. Ogawa, H. linuma, H. Suda, K. Ukita, T. Nagatsu, M. Kato, H. Umezawa, *J. Antibiotics* **1973**, *26*, 162–167.
[11] F. Chimenti, R. Fioravanti, A. Bolasco, P. Chimenti, D. Secci, F. Rossi, M. Yáñez, F. Orallo, F. S. Alcaro, *J. Med. Chem*. **2009**, *52*, 2818–2824.
[12] N. Morales-Camilo, C. O. Salas, C. Sanhueza, C. Espinosa-Bustos, M. Reyes-Parada, F. Gonzalez-Salas, C. Sanhauez, C. Espinosa-Bustos, S. Sepulveda-Boza, M. Reyes-Parada, F. Gonzalez-Nilo, M. Caroli-Rezende, A. Fierro, *Chem. Biol. Drug Des*. **2015**, *85*, 685–695.
[13] B. Mathew, G. E. Mathew, G. Uçar, I. Baysal, J. Suresh, J. K. Vilapurathu, A. Prakasan, J. K. Suresh, A. Thomas, *Bioorg. Chem*. **2015**, *62*, 22–29.
[14] J. W. Choi, B. K. Jang, N. Cho, J. H. Park, S. K. Yeon, E. J. Ju, Y. S. Lee, G. Han, A. M. Pae, D. J. Kim, K.D. Park, *Bioorg. Med. Chem*. **2015**, *23*, 6486–6496.
[15] H. Hammuda, R. Shalaby, S. Rovida, D. E. Edmondson, C. Binda, A. Khali, *Eur. J. Med. Chem*. **2016**, *114*, 162–169.
[16] S. J. Robinson, J. P. Petzer, A. Petzer, J. J. Bergh, A. C. U. Lourens, *Bioorg. Med. Chem. Lett*. **2013**, *23*, 4985–4989.
[17] G. Jo, S. Ahn, B. G. Kim, H. R. Park, Y. H. Kim, H. A. Choo, D. Koh, Y. Chong, J. H. Ahn, Y. Lim, *Bioorg. Med. Chem*. **2013**, *21*, 7890–7897.
[18] S. Zaib, S. U. F. Rizvi, S. Aslam, M. Ahmad, S. M. A. Abid, M. al-Rashida, J. Iqbal, *Med. Chem*. **2015**, *11*, 580–589.
[19] S. Zaib, S. U. F. Rizvi, S. Aslam, M. Ahmad, M. al-Rashida, J. Iqbal, *Med. Chem*. **2015**, *11*, 497–505.
[20] C. Minders, J. P. Petzer, A. Petzer, A. C. U. Lourens, *Bioorg. Med. Chem. Lett*. **2015**, *25*, 5270–5276.
[21] B. Mathew, G. Uçar, S. Y. Ciftci, I. Baysal, J. Suresh, G. E. Mathew, J. K. Vilapurathu, N. A. Moosa, N. Pullarottil, L. Viswam, A. Haridas, F. Fathima, *Lett. Org. Chem*. **2015**, *12*, 605–613.
[22] B. Mathew, A. Haridas, G. Uçar, I. Baysal, M. Joy, G. E. Mathew, B. Lakshmanan, V. Jayaprakash, *ChemMedChem* **2016**, *11*, 1161–1171.
[23] B. Mathew, A. Haridas, G. Uçar, I. Baysal, A. A. Adeniyi, M. E. S. Soliman, M. Joy, G. E. Mathew, B. Lakshmanan, V. Jayaprakash, *Int. J. Biol. Macromol*. **2016**. doi: 10.1016/j.ijbiomac.2016.05.110
[24] B. Mathew, A. Haridas, J. Suresh, G. E. Mathew, G. Ucar, V. Jayaprakash, *Cent. Nerv. Syst. Agents Med. Chem*. **2016**, *16*, 120–136.
[25] Z. V. Chirkova, M. V. Kabanova, S. I. Filimonov, I. G. Abramov, A. Petzer, J. P. Petzer, S. I. Firgang, K. Y. Suponitsky, *Bioorg. Med. Chem. Lett*. **2015**, *25*, 1206–1211.
[26] C. S. Passos, C. A. Simões-Pires, A. Nurisso, T. C. Soldi, L. Kato, C. M. A. de Oliveira, E. O. de Faria, L. Marcourt, C. Gottfried, P. A. Carrupt, A. T. Henriques, *Phytochemistry* **2013**, *86*, 8–20.
[27] L. H. Prins, J. P. Petzer, S. F. Malan, *Eur. J. Med. Chem*. **2010**, *45*, 4458–4466.
[28] N. T. Tzvetkov, S. Hinz, P. Kuppers, M. Gastreich, M. C. E. Muller, *J. Med. Chem*. **2014**, *57*, 6679.
[29] R. K. P. Tripathi, S. Krishnamurthy, S. R. Ayyannan, *ChemMedChem* **2016**, *11*, 119–132.
[30] M. C. Anderson, F. Hasan, J. M. McCrodden, K. F. Tipton, *Neurochem. Res*. **1993**, *18*, 1145–1149.
[31] M. Yáñez, N. Fraiz, E. Cano, F. Orallo, *Biochem. Biophys. Res. Commun*. **2006**, *344*, 688–695.
[32] F. Chimenti, E. Maccioni, D. Secci, A. Bolasco, P. Chimenti, A. Granese, S. Carradori, S. Alcaro, F. Ortuso, M. Yáñez, *J. Med. Chem*. **2008**, *51*, 4874–4880.
[33] B. Mathew, J. Suresh, S. Anbazhagan, G. E. Mathew, *Cent. Nerv. Syst. Agents Med. Chem*. **2013**, *13*, 195–206.
[34] L. J. Legoabe, A. Petzer, J. P. Petzer, *Chem. Biol. Drug Des*. **2015**, *86*, 895–904.
[35] M. Löhle, A. Storch, *Basal Ganglia* **2012**, *2*, S33–S40.
[36] L. Di, E. H. Kerns, K. Fan, O. J. McConnell, G. T. Carter, *Eur. J. Med. Chem*. **2003**, *38*, 223–232.
[37] N. J. Miller, C. A. Rice-Evans, *Free Radical Res*. **1997**, *26*, 195–199.
[38] Z. M. Wang, X. M. Li, G. M. Xue, W. Xu, X. B. Wang, L. Y. Kong, *RSC Adv*. **2015**, *5*, 104122–104137.
[39] C. Binda, J. Wang, L. Pisani, C. Caccia, A. Carrotti, P. Salvati, D. E. Edmondson, A. Mattevi, *J. Med. Chem*. **2007**, *50*, 5848–5852.
[40] L. Legoabe, J. Kruger, A. Petzer, J. J. Bergh, J. P. Petzer, *Eur. J. Med. Chem*. **2011**, *46*, 5162–5174.
[41] D. Kumar, N. M. Kumar, K. Akamatsu, E. Kusaka, H. Harada, T. Ito, *Bioorg. Med. Chem. Lett*. **2010**, *20*, 3016–3919.
[42] M. M. Bradford, *Anal. Biochem*. **1976**, *72*, 248–254.
[43] A. Petzer, A, Pienaar, J. P. Petzer, *Life Sci*. **2013**, *93*, 283–287.
[44] M. B. Hansen, S. E. Nielsen, K. Berg, *J. Immunol. Meth*. **1989**, *119*, 203–210.
[45] C. F. Wu, R. Bertorelli, M. Sacconi, G. Pepeu, S. Consolo, *Neurobiol. Aging* **1988**, *9*, 357–361.
[46] G. M. Morris, R. Huey, W. Lindstrom, M. F. Sanner, R. K. Belew, D. S. Goodsell, A. J. Olson, *J. Comput. Chem*. **2009**, *30*, 2785–2791.
[47] L. De Colibus, M. Li, C. Binda, A. Lustig, D. E. Edmondson, A. Mattevi, *Proc. Natl. Acad. Sci. USA* **2005**, *102*, 12684–12689.
[48] B. V. Nayak, S. Ciftci-Yabanoglu, S. Bhakat, A. K. Timiri, B. NSinha, G. Ucar, M. E. S. Soliman, V. Jayaprakash, *Bioorg. Chem*. **2015**, *58*, 72–80.
[49] A. W. Schuttelkopf, D. M. van Aalten, *Acta Crystallogr. D Biol. Crystallogr*. **2004**, *60*, 1355–1363.
[50] B. V. Nayak, S. Ciftci-Yabanoglu, S. S. Jadav, M. Jagrat, B. N. Sinha, G. Ucar, V. Jayaprakash, *Eur. J. Med. Chem*. **2013**, *69*, 762–767.